POLITECNICO DI TORINO
Repository ISTITUZIONALE

Accurate stress fields of post-buckled laminated composite beams accounting for various kinematics

Original
Accurate stress fields of post-buckled laminated composite beams accounting for various kinematics / Wu, Bin; Pagani, A.; Filippi, M.; Chen, W. Q.; Carrera, E.. - In: INTERNATIONAL JOURNAL OF NON-LINEAR MECHANICS. - ISSN 0020-7462. - 111:(2019), pp. 60-71. [10.1016/j.ijnonlinmec.2019.02.002]

Availability:
This version is available at: 11583/2729220 since: 2019-03-26T10:37:28Z

Publisher:
Elsevier Ltd

Published
DOI:10.1016/j.ijnonlinmec.2019.02.002

Terms of use:

This article is made available under terms and conditions as specified in the corresponding bibliographic description in the repository

Publisher copyright
Elsevier postprint/Author's Accepted Manuscript

© 2019. This manuscript version is made available under the CC-BY-NC-ND 4.0 license
http://creativecommons.org/licenses/by-nc-nd/4.0/.The final authenticated version is available online at:
http://dx.doi.org/10.1016/j.ijnonlinmec.2019.02.002

(Article begins on next page)

18 April 2024

Accurate stress fields of post-buckled laminated composite beams accounting for various kinematics

B. Wu[a], A. Pagani[a,*], M. Filippi[a], W.Q. Chen[b,†], E. Carrera[a,‡]

[a]Mul^2 Group, Department of Mechanical and Aerospace Engineering, Politecnico di Torino, 10129 Torino, Italy;

[b]Department of Engineering Mechanics, Zhejiang University, 310027 Hangzhou, China.

Abstract: Highly flexible laminated composite structures, prone to suffering large-deflection and post-buckling, have been successfully employed in a number of scenarios. Therefore, accurate predictions of their stress distributions in the geometrically nonlinear analysis are of paramount importance for their design and failure evaluation. In this paper, for composite beams subjected to large-deflection and post-buckling, we investigate the effectiveness of different geometrically nonlinear strain approximations for the description of their nonlinear static response and for the determination of stress distributions. For this purpose, a unified formulation of geometrically nonlinear refined beam theory based on the Carrera Unified Formulation (CUF) and a total Lagrangian approach constitutes the basis of our analysis. Accordingly, various kinematics of one-dimensional structures are formulated via an appropriate index notation and an arbitrary cross-section expansion of the generalized variables, leading to lower- to higher-order beam models with only pure displacement variables for laminated composite beams. In view of the intrinsic scalable nature of CUF and by exploiting the principle of virtual work and a finite element approximation, nonlinear governing equations corresponding to various nonlinear strain assumptions can be straightforwardly and easily formulated in terms of fundamental nuclei, which are independent of the theory approximation order. Several numerical assessments are conducted, including large-deflection and post-buckling analyses of asymmetric and symmetric laminated beams under compression loadings. The numerical solutions are solved by using a Newton-Raphson linearization scheme along with a path-following method based on the arc-length constraint. Our numerical findings demonstrate the capabilities of the CUF model to calculate the large-deflection and post-buckling equilibrium curves as well as the stress distributions with high accuracy, which could be a basis to assess the validation ranges of various kinematics and different nonlinear strain approximations.

Keywords: Carrera Unified Formulation; Geometrical nonlinearities; Post-buckling; Composite beams; Accurate stress fields; Strain approximations.

---

*Assistant professor. E-mail: alfonso.pagani@polito.it

†Professor of Engineering Mechanics. E-mail: chenwq@zju.edu.cn

‡Professor of Aerospace Structures and Aeroelasticity. E-mail: erasmo.carrera@polito.it

1 Introduction

Owing to their superior advantages such as high strength-to-weight and stiffness-to-weight ratios, laminated composite structures have been of great interest for many decades, with widespread applications in numerous areas, especially in the aeronautical and aerospace industry. Consequently, a large number of theories have been developed in order to improve those obsolete models that were originally established for metallic components, and to understand their structural behaviors such as deformation characteristics and stress/strain distributions. Interested readers can refer to the bibliographic review works by Carrera [1] and Kapania and Raciti [2, 3], which addressed in a comprehensive manner the modeling and analysis of composite laminates for beam and plate/shell structures in the linear regime. In contrast, highly flexible structures, susceptible to suffering large displacements and rotations, are widely employed in various engineering structural components, as for example, wing structures, space antennas and rotor blades in aeronautical engineering, robotic arms in mechanical engineering, hulls of submarines in naval industry, tubes and pipelines for liquid or gas transportation in chemical industry, etc. Moreover, complex soft tissues and organs as well as advanced biological instrument are usually made of highly flexible structures. A recent literature review on the modeling of these nonlinear plate/shell structures in the application of bioengineering can be seen in the valuable monograph by Amabili [4]. As a result, the elastic, geometrical nonlinear analysis of laminated composite structures has always been a fundamental topic in structural mechanics. Accurate predictions of stress distributions (especially the interlaminar stresses) in the geometrically nonlinear (including large-deflection and post-buckling) analysis are challenging but essential for the design and failure evaluation of these composite structures.

Nowadays, considerable attention has been focusing on the problem of how to establish an excellent theory to exactly determine the three-dimensional (3D) stress fields. It is well known that owing to the neglect of transverse shear effects, the classical Euler-Bernoulli beam theory (classical lamination theory, CLT) [5] is too limiting for the analysis of laminated composite beams. Although the Timoshenko beam theory [6], the extension of which to the analysis of laminates is known as the first-order shear deformation theory (FSDT), assumes a uniform shear distribution across the cross-section together with the rotatory inertia effects, it is not adequate for forecasting local stress-strain characteristics of the composite beams [7]. Therefore, a variety of higher-order shear deformation theories (HSDT) that improve CLT and FSDT have been proposed for the enhancement of solutions in laminated composite structures [8, 9, 10, 11, 12, 13, 14]. Inherently, these theories, assuming the laminate as an equivalent single layer (ESL) whose properties can be obtained by homogenization techniques, can be derived by introducing gradually the high-order terms into the in-plane and transverse displacement components and have the advantage that the number of the unknowns is independent of the number of the layers [15]. Nevertheless, the failure of HSDT or ESL models to accurately predict the displacement and stress fields is mainly due to the fact that these theories could not fulfill the interlaminar stress continuity conditions at each interface and are not able to describe the so-called zig-zag shape distributions [7, 16] of displacement fields along the laminate thickness [15, 17]. Recently, the Murakami zig-zag function (MZZF) [18] was used to provide a valuable tool to enhance the performance of both CLT and HSDT [19]. Specifically, the zig-zag effect could be easily included into the existing CLT and HSDT for laminated structures [19]. It is worth noting that, based on the Reissner's mixed variational theorem [20, 21] and in the framework of ESL models, C^0 Reissner-Mindlin laminated plate elements including both the zig-zag distribution along the thickness direction of in-

plane displacements and the interlaminar continuity for transverse shear stresses, i.e. RMZC (Reissner-Mindlin Zig-zag Continuity) elements, were established [22].

Furthermore, in order to generate more accurate and realistic distributions of strains and stresses, the layer-wise theories (LWT), which consider each layer as a single lamina with different material properties leading to the increase of the number of the unknowns, can capture well the zig-zag form of the displacement fields that are matched at each interface [23, 24, 25]. Based on the Reissner's mixed variational theorem [20, 21], a layer-wise mixed theory [26] was developed to furnish a better description of the in-plane and out-of-plane response of laminated structures with respect to existing ESL theories and LWT. Particularly, the layer-wise mixed theory satisfies *a priori* the continuity of transverse shear and normal stress components at interfaces and describes the transverse shear and normal stress fields with excellent accuracy [26].

It should be noted that various advances with emphasis on the accuracy improvement of stress field distributions can be found in the literature. For instance, the additional enhancement functions such as transverse Hermite polynomials were introduced into the zig-zag higher-order C^1 formulations for the displacements to enforce the continuity of the transverse shear stresses [27]. Nonetheless, their generalization to more complex problems (i.e. robustness) still remains questionable. In contrast to the displacement-based elements exhibiting over rigidity, the hybrid stress elements with high performance [28, 29, 30] were developed for better description of stress distributions but their developments are complicated and limited to the linear analysis. A good summary of the evolution regarding the 3D stress field calculation can be seen in the work [31], which demonstrated an extremely enlightening discussion of the pros and cons of the above-mentioned analytical, semi-analytical or numerical approaches. The same authors also presented an efficient 3D Hybrid-EAS (enhanced assumed strain) solid element formulation to accurately predict interlaminar stresses in thick laminated beams and plates/shells based on the mixed three-field Fraeijs de Veubeke-Hu-Washizu (FHW) functional principle [31].

The presence of geometrical nonlinearities of highly flexible structures greatly increases the difficulties of finding analytical and even numerical solutions, as a result of which only a few results are available concerning the distributions of stress and displacement components along the thickness direction of laminated structures in the geometrically nonlinear scenario. In the framework of ESL models, laminated finite elements for composite beams and plates/shells were formulated based on the total Lagrangian kinematic description to carry out the geometrically nonlinear analysis [32, 33], which demonstrated good stress distributions even for complex materials in the case of large displacements. The same authors [34], furthermore, included the zig-zag effect on the distributions of displacements and transverse stresses of laminated structures into the geometrically nonlinear laminated finite elements developed in [32, 33]. In the framework of LWT models, a positional unconstrained vector layer-wise FEM formulation accounting for the geometrical nonlinearities were established for laminated structures in order to obtain an accurate determination of transverse stresses and eliminate the ill-conditioning of stiffness matrix for thin elements [35]. However, their mathematical derivations are in some sense cumbersome and not easily generalized. Additionally, it should be emphasized that the aforementioned works are primarily devoted to discussing the stress distributions in the large-deflection fields before buckling and post-buckling. In fact, some structural components (such as fuselage, wing, and stabilizer panels) of current aircraft are designed to have a post-buckling strength. Evidently, a better understanding of the post-buckling behavior of laminated composite and a more accurate prediction of the stress distributions in the post-buckling case constitute an essential requirement toward ra-

tional employment of their strength. Based on the von Kármán assumption in conjunction with a mixed two-dimensional (2D) mechanical model [22], the local characteristics of displacement and stress distributions for laminated plates were numerically investigated in the large-deflection and post-buckling scenarios, where the RMZC model was also developed to describe the zig-zag form for the in-plane displacement components and the interlaminar continuity of the transverse shear stress components [15]. To the authors' best knowledge, no results are available from the open literature regarding the accurate prediction of stress distributions of laminates in the post-buckling regime based on the 3D full geometrically nonlinear analysis, which takes into consideration all nonlinear terms of the Green-Lagrange strain tensor.

In addition to the precise calculation of displacement and stress/strain distributions, the accurate description of large-deflection, buckling and post-buckling nonlinear response also plays a crucial role in the design, manufacturing, and application of composite laminates. As a matter of fact, as the extension of the Euler-Bernoulli and Timoshenko beam theories, contributions to the development of FSDT, HSDT as well as refined beam theories in the geometrically nonlinear scenario have been made so as to effectively analyze the large-deflection, buckling and post-buckling response [36, 37, 38, 39, 40, 41, 13]. The literature about this subject is enormous, and a detailed discussion on nonlinear formulations of composite beam structures falls outside the scope of this paper. It is worthy to mention that most of the research works in the literature made use of the von Kármán nonlinear strain approximation to assess the load-carrying capability of highly flexible composite structures. As commented by Carrera and Parisch [42] in the evaluation of geometrically nonlinear effects of laminated composite shells, the von Kármán approximation could obtain good accuracy in the thin shell case when deflections are of the same order of magnitude of the thickness, while such accuracy could be not confirmed for the thick structures. Furthermore, the same authors pointed out that the error made by the von Kármán approximation is more evident in the case of shear loadings in which the deformation exhibits large rotations. Moreover, in the geometrically nonlinear analysis of laminated cylindrical panels, Kim and Chaudhuri [43] demonstrated that the von Kármán nonlinear strain approximation overestimates the transverse displacements, especially in the advanced nonlinear regime. As far as the authors' knowledge goes, the accuracy of different geometrically nonlinear strain approximations for laminated beam structures and their related effects on nonlinear stress distributions (especially the von Kármán approximation) have not been studied yet in the literature.

As a consequence, the primary objectives of the present investigation are: (1) to compare and determine the effectiveness of various geometrically nonlinear strain assumptions for the analysis of large-deflection and post-buckling nonlinear response for composite beams; (2) to accurately predict their stress distributions in the large-deflection and post-buckling regime and compare the prediction results based on different nonlinear strain approximations. The geometrically nonlinear analysis in this investigation is based on the Carrera Unified Formulation (CUF), which has been recently extended to geometrically nonlinear analyses for both metallic and composite beam structures [44, 45]. According to CUF [46, 47], any structural theory could degenerate into a generalized kinematics by utilizing an appropriate expansion of the generalized variables (such as Lagrange and Taylor expansions). In this manner, the nonlinear governing equations and the related finite element arrays of the generic geometrically-exact composite beam theory can be expressed in terms of *fundamental nuclei*, which represent the basic building blocks allowing for the straightforward generation of lower- and higher-order finite beam elements. Over the last few years, CUF has been employed to solve many engineering problems, including aerospace constructions [48], civil engineering

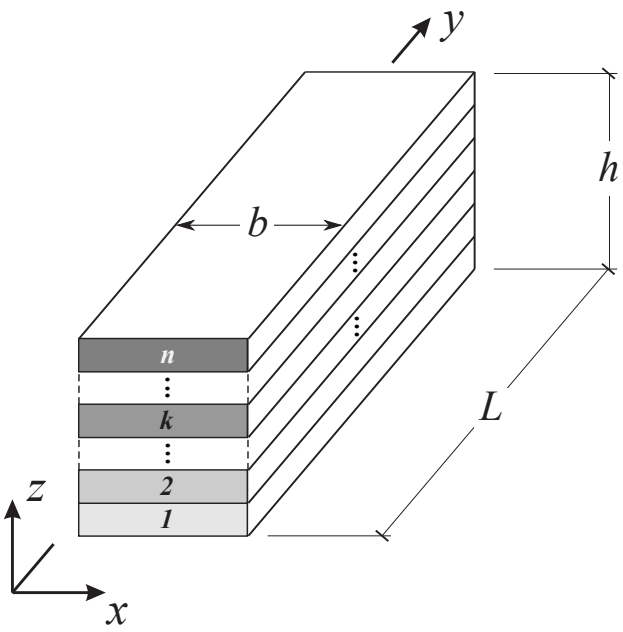

Figure 1: n-ply laminated composite beam and related Cartesian coordinate system.

structures [49], rotating blades and rotors [50], multi-field problems [51], and free vibration analysis [52], among the others. It should be emphasized that, owing to its intrinsic scalable nature, different nonlinear strain approximations can be automatically and opportunely incorporated by using CUF.

2 Unified finite beam element

2.1 Preliminary formulations

Consider a n-ply laminated composite beam structure of width b, thickness h, and length L displayed in Fig. 1, with each layer being made of linear elastic monoclinic material in the $x-y$ plane (e.g., orthotropic fiber-matrix lamina with fiber orientation angle equal to θ with respect to the z-axis). The 3D displacement vector ($\mathbf{u}$) of a given point in the composite beam is

$$\mathbf{u}(x,y,z) = \left\{ \begin{array}{ccc} u_x & u_y & u_z \end{array} \right\}^{\mathrm{T}} \tag{1}$$

The stress ($\boldsymbol{\sigma}$)-strain ($\boldsymbol{\epsilon}$) constitutive relations for these materials with monoclinic symmetry can be expressed as

$$\boldsymbol{\sigma} = \tilde{\mathbf{C}}\boldsymbol{\epsilon} \tag{2}$$

where the stress ($\boldsymbol{\sigma}$) and strain ($\boldsymbol{\epsilon}$) can be written as

$$\boldsymbol{\sigma} = \left\{ \begin{array}{cccccc} \sigma_{xx} & \sigma_{yy} & \sigma_{zz} & \sigma_{xz} & \sigma_{yz} & \sigma_{xy} \end{array} \right\}^{\mathrm{T}}, \quad \boldsymbol{\epsilon} = \left\{ \begin{array}{cccccc} \epsilon_{xx} & \epsilon_{yy} & \epsilon_{zz} & \epsilon_{xz} & \epsilon_{yz} & \epsilon_{xy} \end{array} \right\}^{\mathrm{T}} \tag{3}$$

and the material elastic matrix $\tilde{\mathbf{C}}$ is

$$\tilde{\mathbf{C}} = \begin{bmatrix} \tilde{C}_{11} & \tilde{C}_{12} & \tilde{C}_{13} & 0 & 0 & \tilde{C}_{16} \\ & \tilde{C}_{22} & \tilde{C}_{23} & 0 & 0 & \tilde{C}_{26} \\ & & \tilde{C}_{33} & 0 & 0 & \tilde{C}_{36} \\ & & & \tilde{C}_{44} & \tilde{C}_{45} & 0 \\ & & & & \tilde{C}_{55} & 0 \\ \text{sym.} & & & & & \tilde{C}_{66} \end{bmatrix} \tag{4}$$

Note that the elastic coefficients $\tilde{C}_{ij}$ are functions of the elastic moduli along the longitudinal and transverse directions of the fiber, the shear moduli, the Poisson's ratios, and the fiber orientation angle. Their specific expressions are omitted here for simplicity, but can be found in many reference texts, such as [53].

For many problems of large displacement and rotation analysis as well as elastic post-buckling analysis, the displacement derivatives are finite and the inclusion of their high-order terms into the geometrical relations is of practical importance for accurately predicting the geometrically nonlinear response and the stress field distributions. In fact, the *total Lagrangian* formulations are generally utilized to describe the pure geometrically nonlinear problems based on a natural undeformed state to which the structure will recover if unloaded. In contrast to the *Eulerian* and *updated Lagrangian* formulations, strains are expressed in terms of the undeformed configuration in the total Lagrangian description. This aspect entails a number of advantages when a total Lagrangian formulation is employed along with a numerical incremental solution scheme [32, 35, 54]: (1) Theoretically, there exists no error accumulation due to the independence of the accuracy at the current solution step on the solution at the previous step; (2) There is no necessity to conduct any coordinate transformation of stress and strain components during iteration; (3) If the implemented approach is convergent, large loading steps and reverse analysis can be allowed with no loss of accuracy.

In the proposed total Lagrangian description, the Green-Lagrange strain tensor will be used to measure the geometrically nonlinear strain. The reasons are that Green-Lagrange strains vanish for rigid body rotations (this is not true in the case of engineering strains) and these strains are work-conjugate to the second Piola-Kirchoff stresses. Specifically, the Green-Lagrange strain components can be defined as:

$$\boldsymbol{\epsilon} = \boldsymbol{\epsilon}_l + \boldsymbol{\epsilon}_{nl} = (\mathbf{b}_l + \mathbf{b}_{nl})\mathbf{u} \tag{5}$$

where the linear and nonlinear differential operators $\mathbf{b}_l$ and $\mathbf{b}_{nl}$ are defined as:

$$\mathbf{b}_l = \begin{bmatrix} 0 & \partial_y & 0 \\ \partial_x & 0 & 0 \\ 0 & 0 & \partial_z \\ \partial_z & 0 & \partial_x \\ 0 & \partial_z & \partial_y \\ \partial_y & \partial_x & 0 \end{bmatrix}, \qquad \mathbf{b}_{nl} = \begin{bmatrix} \frac{1}{2}(\partial_y)^2 & \frac{1}{2}(\partial_y)^2 & \frac{1}{2}(\partial_y)^2 \\ \frac{1}{2}(\partial_x)^2 & \frac{1}{2}(\partial_x)^2 & \frac{1}{2}(\partial_x)^2 \\ \frac{1}{2}(\partial_z)^2 & \frac{1}{2}(\partial_z)^2 & \frac{1}{2}(\partial_z)^2 \\ \partial_x\,\partial_z & \partial_x\,\partial_z & \partial_x\,\partial_z \\ \partial_y\,\partial_z & \partial_y\,\partial_z & \partial_y\,\partial_z \\ \partial_x\,\partial_y & \partial_x\,\partial_y & \partial_x\,\partial_y \end{bmatrix} \tag{6}$$

in which $\partial_x = \partial(\cdot)/\partial x$, $\partial_y = \partial(\cdot)/\partial y$, and $\partial_z = \partial(\cdot)/\partial z$.

It should be emphasized that large displacements and rotations may *induce* coupling phenomena among bending, extension, shear, and torsion of structures. Consequently, it is necessary to account for the 3D full Green-Lagrange strains shown in Eq. (6). Over the last decades, on the other hand, many simplified geometrically nonlinear models have been established for two-dimensional (2D) and one-dimensional (1D) structures from the 3D full geometrical relations, among which the von Kármán nonlinear strain approximation for plates is the well-known model, see [55]. Inherently, the von Kármán theory for 2D thin plates/shells with moderate rotations hypothesizes that the nonlinear terms of Eq. (6) that cannot be discarded

are those associated with the in-plane partial derivatives of the transverse displacement, which means that the only non-zero terms of geometrically nonlinear strains are

$$\epsilon_{xx_{nl}} = \frac{1}{2}(u_{z,x})^2, \quad \epsilon_{yy_{nl}} = \frac{1}{2}(u_{z,y})^2, \quad \epsilon_{xy_{nl}} = u_{z,x}u_{z,y} \tag{7}$$

where comma denotes the partial derivative and the z-axis is placed along the thickness direction of the plates/shells. Applying von Kármán assumptions to the case of 1D beams, one can obtain the only non-zero component of the nonlinear strain vector as:

$$\epsilon_{yy_{nl}} = \frac{1}{2}(u_{z,y})^2 \tag{8}$$

where the undeformed beam axis is located along the y-axis as shown in Fig. 1. Although numerous research works are based on the von Kármán model, it is well known that it cannot even properly capture the moderate rotations [54].

In this work, we will study the effects of different geometrically nonlinear strain assumptions on the geometrically nonlinear response and the stress field distributions of the flexible laminated composite beams in the case of large-deflection and post-buckling. For this purpose, the Carrera Unified Formulation (CUF) will be employed to formulate the nonlinear governing equations of composite beams. In fact, owing to the superior advantages of CUF such as the scalable nature, one can develop conveniently the nonlinear governing equations for beam, plate and shell structures in a unified manner. Furthermore, by eventually vanishing or adding the corresponding nonlinear terms into the CUF fundamental nuclei (the basic building blocks of the secant and tangent stiffness matrices), we can obtain different geometrically nonlinear models, such as the 3D full Green-Lagrange strain model (Eq. (6)) and the simplified von Kármán model (Eqs. (7) and (8)).

2.2 CUF and finite element approximation

Within the framework of CUF, the 3D displacement field $\mathbf{u}(x, y, z)$ can be expanded in terms of the primary unknowns. Specifically, for the 1D beam theory, we have:

$$\mathbf{u}(x, y, z) = F_s(x, z)\mathbf{u}_s(y), \qquad s = 1, 2, \cdots, M \tag{9}$$

where F_s are the expansion functions of the coordinates x and z on the cross-section, $\mathbf{u}_s$ is the vector of the *generalized* displacements along the beam axis y, M represents the number of the expansion terms, and the repeated subscript s indicates summation. The choice of F_s determines the class of the 1D CUF model that is to be adopted.

In this paper, we will consider both the Taylor and Lagrange polynomials as F_s cross-sectional functions. The resulting beam theories are known as Taylor expansion (TE) and Lagrange expansion (LE) CUF models in the literature [47]. Specifically, the first-order and second-order Taylor expansions, four-node bilinear (L4), nine-node quadratic (L9), and 16-node cubic (L16) Lagrange expansions are exploited on the cross-section of the laminated beams. Compared with the TE beam models, the LE beam models are equipped with only pure displacement variables, layer-dependent unknowns and piece-wise refined kinematics. Additionally, the higher-order LE layer-wise formulation in the context of CUF can predict the results of stress distributions more accurately than the TE predictions, which will be demonstrated in Sec. 5. The TE and LE functions F_s are not presented here for brevity. For more details about the descriptions of TE and LE CUF models as well as the formulation of layer-wise models, the interested reader is referred to the texts [46] and [47].

For the sake of generality, the Finite Element Method (FEM) is adopted to discretize the structure along the y-axis. Therefore, the generalized displacement vector $\mathbf{u}_s(y)$ is approximated as follows:

$$\mathbf{u}_s(y) = N_j(y)\mathbf{q}_{sj} \qquad j = 1, 2, \ldots, p+1 \tag{10}$$

where N_j represents the j-th shape function, p is the order of the shape functions and j indicates summation. The vector of the FE nodal parameters $\mathbf{q}_{sj}$ is defined as

$$\mathbf{q}_{sj} = \left\{ \begin{array}{ccc} q_{x_{sj}} & q_{y_{sj}} & q_{z_{sj}} \end{array} \right\}^{\mathrm{T}} \tag{11}$$

The specific expressions of the shape functions N_j are not shown here for simplicity, which can be found in many reference books about FEMs, for instance in Bathe [56]. In this work, the classical 1D four-node cubic finite elements will be adopted for the shape function along the y-axis. It is worth noting that the choice of the cross-section polynomials for various kinematics is completely independent of that of the beam finite element along the beam axis.

3 Nonlinear governing equations

As is known to all, nonlinear static equilibrium equations can be derived based on the principle of virtual work, which states that for arbitrary infinitesimal virtual displacement satisfying the prescribed geometrical constraints, the virtual variation of internal strain energy (δL_{int}) must be equal to the virtual variation of the work of external loadings (δL_{ext}), i.e.,

$$\delta L_{\mathrm{int}} = \delta L_{\mathrm{ext}} \tag{12}$$

Large displacement/rotation analysis of elastic systems leads to complex nonlinear differential problems which are difficult to solve analytically. However, if FEM (Eq. (10)) and CUF (Eq. (9)) are employed, the nonlinear equilibrium equation (12) of the structure can be expressed as a system of nonlinear algebraic equations which will be derived below.

The virtual variation of the strain energy, for example, can be written as

$$\delta L_{\mathrm{int}} = < \delta \boldsymbol{\epsilon}^{\mathrm{T}} \boldsymbol{\sigma} > \tag{13}$$

where $< (\cdot) > = \int_V (\cdot)\, dV$ and $V = \Omega \times L$ is the initial volume of the beam structure. Making use of Eqs. (9) and (10), we can express the strain vector $\boldsymbol{\epsilon}$ in Eq. (5) and its virtual variation $\delta\boldsymbol{\epsilon}$ in terms of the generalized FE nodal unknowns $\mathbf{q}_{sj}$ and $\delta\mathbf{q}_{\tau i}$ as

$$\boldsymbol{\epsilon} = (\mathbf{B}_l^{sj} + \mathbf{B}_{nl}^{sj})\mathbf{q}_{sj}, \qquad \delta\boldsymbol{\epsilon} = (\mathbf{B}_l^{\tau i} + 2\mathbf{B}_{nl}^{\tau i})\delta\mathbf{q}_{\tau i} \tag{14}$$

where the two matrices $\mathbf{B}_l^{sj}$ and $\mathbf{B}_{nl}^{sj}$ of linear and nonlinear geometrical relations are given by

$$\mathbf{B}_l^{sj} = \mathbf{b}_l(F_s\, N_j) = \begin{bmatrix} F_{s,x}N_j & 0 & 0 \\ 0 & F_s N_{j,y} & 0 \\ 0 & 0 & F_{s,z}N_j \\ F_{s,z}N_j & 0 & F_{s,x}N_j \\ 0 & F_{s,z}N_j & F_s N_{j,y} \\ F_s N_{j,y} & F_{s,x}N_j & 0 \end{bmatrix} \tag{15}$$

and

$$\mathbf{B}_{nl}^{sj} = \frac{1}{2}\begin{bmatrix} u_{x,x}F_{s,x}N_j & u_{y,x}F_{s,x}N_j & u_{z,x}F_{s,x}N_j \\ u_{x,y}F_sN_{j,y} & u_{y,y}F_sN_{j,y} & u_{z,y}F_sN_{j,y} \\ u_{x,z}F_{s,z}N_j & u_{y,z}F_{s,z}N_j & u_{z,z}F_{s,z}N_j \\ u_{x,x}F_{s,z}N_j + u_{x,z}F_{s,x}N_j & u_{y,x}F_{s,z}N_j + u_{y,z}F_{s,x}N_j & u_{z,x}F_{s,z}N_j + u_{z,z}F_{s,x}N_j \\ u_{x,y}F_{s,z}N_j + u_{x,z}F_sN_{j,y} & u_{y,y}F_{s,z}N_j + u_{y,z}F_sN_{j,y} & u_{z,y}F_{s,z}N_j + u_{z,z}F_sN_{j,y} \\ u_{x,x}F_sN_{j,y} + u_{x,y}F_{s,x}N_j & u_{y,x}F_sN_{j,y} + u_{y,y}F_{s,x}N_j & u_{z,x}F_sN_{j,y} + u_{z,y}F_{s,x}N_j \end{bmatrix} \tag{16}$$

The other two matrices $\mathbf{B}_l^{\tau i}$ and $\mathbf{B}_{nl}^{\tau i}$ can be obtained by replacing the indices s and j with τ and i in Eqs. (15) and (16). It should be pointed out that Eq. (16) is valid for the 3D full Green-Lagrange strains in Eq. (6), which can be easily modified to account for different geometrically nonlinear assumptions. For example, for the 1D von Kármán model with the only non-zero nonlinear strain component given in Eq. (8), the geometrical matrix operator $\mathbf{B}_{nl}^{sj}$ will become

$$\left[\mathbf{B}_{nl}^{sj}\right]^{\text{1D-VK}} = \frac{1}{2}\begin{bmatrix} 0 & 0 & 0 \\ 0 & 0 & u_{z,y}F_sN_{j,y} \\ 0 & 0 & 0 \\ 0 & 0 & 0 \\ 0 & 0 & 0 \\ 0 & 0 & 0 \end{bmatrix} \tag{17}$$

Substituting these geometric relations (Eqs. (14)) into Eq. (13) and using the constitutive equation (2) and CUF (Eqs. (9) and (10)) yields

$$\delta L_{\text{int}} = \delta \mathbf{q}_{\tau i}^{\mathrm{T}} < \left(\mathbf{B}_l^{\tau i} + 2\,\mathbf{B}_{nl}^{\tau i}\right)^{\mathrm{T}} \tilde{\mathbf{C}} \left(\mathbf{B}_l^{sj} + \mathbf{B}_{nl}^{sj}\right) > \mathbf{q}_{sj} = \delta \mathbf{q}_{\tau i}^{\mathrm{T}} \mathbf{K}_S^{ij\tau s} \mathbf{q}_{sj} \tag{18}$$

where $\mathbf{K}_S^{ij\tau s} = \mathbf{K}_0^{ij\tau s} + \mathbf{K}_{lnl}^{ij\tau s} + \mathbf{K}_{nll}^{ij\tau s} + \mathbf{K}_{nlnl}^{ij\tau s}$ is the *Fundamental Nucleus* (FN) of the *secant* stiffness matrix. Note that $\mathbf{K}_0^{ij\tau s}$ stands for the linear component of $\mathbf{K}_S$, $\mathbf{K}_{lnl}^{ij\tau s}$ and $\mathbf{K}_{nll}^{ij\tau s}$ represent the nonlinear contributions of first order, and $\mathbf{K}_{nlnl}^{ij\tau s}$ contains the nonlinearities of second order [44, 45]. These 3×3 matrices are obviously expressed as

$$\begin{aligned} \mathbf{K}_0^{ij\tau s} &=< (\mathbf{B}_l^{sj})^{\mathrm{T}} \mathbf{C}\, \mathbf{B}_l^{\tau i} > , & \mathbf{K}_{lnl}^{ij\tau s} &=< (\mathbf{B}_l^{sj})^{\mathrm{T}} \mathbf{C}\, \mathbf{B}_{nl}^{\tau i} > \\ \mathbf{K}_{nll}^{ij\tau s} &= 2 < (\mathbf{B}_{nl}^{sj})^{\mathrm{T}} \mathbf{C}\, \mathbf{B}_l^{\tau i} > , & \mathbf{K}_{nlnl}^{ij\tau s} &= 2 < (\mathbf{B}_{nl}^{sj})^{\mathrm{T}} \mathbf{C}\, \mathbf{B}_{nl}^{\tau i} > \end{aligned} \tag{19}$$

The specific expressions of these matrices and the FN of the 3×3 secant stiffness matrix $\mathbf{K}_S^{ij\tau s}$ are not given here for the sake of brevity, which have been presented in the work of Pagani and Carrera [45]. Given the cross-sectional functions ($F_\tau = F_s$, for $\tau = s$) and the axial shape functions ($N_i = N_j$, for $i = j$), the elemental secant stiffness matrix of any arbitrarily refined beam model can be obtained by using the indices $\tau, s = 1, ..., M$ and $i, j = 1, ..., p+1$. In other words, by opportunely choosing various beam kinematics (i.e., by choosing F_τ as well as the number of expansion terms M), we can implement the classical and higher-order beam theories as well as the related secant stiffness matrices in an automatic manner based on the index notation of CUF. In addition, it is evident from the above derivations that,

by properly varying $\mathbf{B}_{nl}^{sj}$, $\mathbf{K}_S^{ij\tau s}$ can be easily scaled to account for different geometrically nonlinear approximations, from the 3D full Green-Lagrange strains (Eq. (6)) to the simplified von Kármán strains (Eq. (8)).

Once the elemental secant stiffness matrix is obtained according to the desirable approximation order and for different assumptions of geometrically nonlinear strains, it can be assembled in the classical way of FEM, see [47]. In fact, after the virtual variation of the external work δL_{ext} is also formulated by $\delta \mathbf{q}_{\tau i}$ (conservative systems are considered in this work) and the finite element assembly procedure in the framework of CUF is conducted, the nonlinear algebraic governing equations can be, thus, obtained from Eq. (12) as

$$\mathbf{K}_S \, \mathbf{q} - \mathbf{p} = \mathbf{0} \tag{20}$$

where $\mathbf{K}_S$, $\mathbf{q}$, and $\mathbf{p}$ are global, assembled finite element arrays of the final structure. For more details about the calculation of the work of external loadings and the related vector of generalized forces $\mathbf{p}$, interested readers are referred to Carrera *et al.* [47].

4 Linearization for the tangent stiffness matrix

In order to conduct the finite element calculation of the nonlinear algebraic governing equations (20), an incremental linearized scheme, typically the Newton-Raphson method (or *tangent method*), has been used by Pagani and Carrera [44, 45] to solve the geometrically nonlinear systems. Based on the Newton-Raphson method, Eq. (20) can be expressed as:

$$\boldsymbol{\varphi}_{res} \equiv \mathbf{K}_S \, \mathbf{q} - \mathbf{p} = \mathbf{0} \tag{21}$$

where $\boldsymbol{\varphi}_{res}$ is the vector of the *residual nodal forces* (unbalanced nodal force vector). Expanding $\boldsymbol{\varphi}_{res}$ of Eq. (21) in Taylor's series about a known solution $(\mathbf{q}, \mathbf{p})$, utilizing the linearization method and omitting the second-order terms, we have

$$\boldsymbol{\varphi}_{res}(\mathbf{q} + \delta\mathbf{q}, \mathbf{p} + \delta\mathbf{p}) = \boldsymbol{\varphi}_{res}(\mathbf{q}, \mathbf{p}) + \frac{\partial \boldsymbol{\varphi}_{res}}{\partial \mathbf{q}} \, \delta\mathbf{q} + \frac{\partial \boldsymbol{\varphi}_{res}}{\partial \mathbf{p}} \, \delta\lambda \, \mathbf{p}_{ref} = \mathbf{0} \tag{22}$$

where $\partial \boldsymbol{\varphi}_{res} / \partial \mathbf{q} = \mathbf{K}_T$ is the *tangent* stiffness matrix and $-\partial \boldsymbol{\varphi}_{res} / \partial \mathbf{p}$ is equal to the unit matrix $\mathbf{I}$. In Eq. (22), it has been envisioned that the load varies directly with the vector of the reference loadings $\mathbf{p}_{ref}$ with a rate of change equal to the load parameter λ, i.e. $\mathbf{p} = \lambda \, \mathbf{p}_{ref}$. Furthermore, it should be emphasized that, since we take the load-scaling parameter λ as a variable, an additional constraint relationship $c(\delta\mathbf{q}, \delta\lambda)$ is required to Eq. (22), which finally leads to

$$\begin{cases} \mathbf{K}_T \, \delta\mathbf{q} = \delta\lambda \, \mathbf{p}_{ref} - \boldsymbol{\varphi}_{res} \\ \\ c(\delta\mathbf{q}, \delta\lambda) = 0 \end{cases} \tag{23}$$

Depending on the constraint equation, different incremental schemes can be implemented. For instance, the constraint relationship $\delta\lambda = 0$ corresponds to a load-control method, while the constraint condition $\delta\mathbf{q} = 0$ represents a displacement-control method. In this work, a path-following constraint equation, which is a function of both displacement and load parameter variations, is employed. Specifically, an arch-length method proposed by Crisfield [57, 58] and later modified by Carrera [59] is utilized in this paper. More explanations about the arch-length method are omitted here and interested readers are referred to the above-mentioned literature.

For the purpose of completeness, it is pointed out that the tangent stiffness matrix $\mathbf{K}_T$ can be derived from the linearization of the nonlinear static equilibrium equation (12) [60]. In the case of conservative loading, the linearization of the virtual variation of external loads vanishes, i.e. $\delta(\delta L_{\text{ext}}) = 0$. Therefore, the only terms to be linearized are the strain-displacement operators and the stress-strain relations. As a matter of fact, linearizing the virtual variation of the internal strain energy can yield

$$\delta(\delta L_{\text{int}}) = < \delta(\delta\boldsymbol{\epsilon}^{\mathrm{T}}\boldsymbol{\sigma}) > = < \delta\boldsymbol{\epsilon}^{\mathrm{T}}\delta\boldsymbol{\sigma} > + < \delta(\delta\boldsymbol{\epsilon}^{\mathrm{T}})\boldsymbol{\sigma} > = \delta\mathbf{q}_{\tau i}^{\mathrm{T}}\mathbf{K}_T^{ij\tau s}\delta\mathbf{q}_{sj} \tag{24}$$

where $\mathbf{K}_T^{ij\tau s} = \mathbf{K}_0^{ij\tau s} + \mathbf{K}_{T_1}^{ij\tau s} + \mathbf{K}_\sigma^{ij\tau s}$, in which $\mathbf{K}_{T_1}^{ij\tau s} = 2\,\mathbf{K}_{lnl}^{ij\tau s} + \mathbf{K}_{nll}^{ij\tau s} + 2\,\mathbf{K}_{nlnl}^{ij\tau s}$, and $\mathbf{K}_\sigma^{ij\tau s}$, arising from the nonlinear form of the strain-displacement relations, is often called the geometrical stiffness [44, 45]. The specific derivation procedure and expressions of $\mathbf{K}_T^{ij\tau s}$ are provided in the work of Pagani and Carrera [45] and not shown here for brevity. Analogous to the case of the secant stiffness matrix, $\mathbf{K}_T^{ij\tau s}$ represents the 3×3 FN and can be used as the basic building block to formulate the tangent stiffness matrix for any higher-order refined beam elements accounting for various kinematics and different nonlinear strain approximations.

It is worth mentioning that unlike the secant stiffness matrix $\mathbf{K}_S$, the tangent stiffness matrix $\mathbf{K}_T$ is symmetric. As Pagani and Carrera [44] pointed out, the main disadvantages of employing $\mathbf{K}_S$ to solve the geometrically nonlinear governing equations (20) is that the generally non-symmetric secant stiffness matrix is not uniquely defined and leads to resolution methods with lower orders of convergence (approximately 1.6 against 2 of tangent methods). Thus, in this work, the tangent stiffness matrix is employed to formulate the linearized iterative scheme while the secant stiffness matrix is exploited merely for evaluating the equilibrium defect and the residual at each iteration. Additionally, we will use the *full* Newton-Raphson method that updates the tangent stiffness matrix at each iteration to carry out the numerical calculations displayed in Sec. 5.

5 Numerical results

In this section, numerical calculations will be conducted for the post-buckling of three-layered symmetric or asymmetric cross-ply beams and the large displacement analysis of two-layered asymmetric composite beams under compression loadings, in order to quantitatively compare the numerical results of various kinematics and determine the validation ranges of different geometrically nonlinear approximations based on the 3D full geometrically nonlinear CUF beam model. If not otherwise stated, 20 cubic finite elements along the longitudinal axis are employed to approximate the solution fields with high accuracy.

5.1 Post-buckling of three-layered composite beams

The first loading case addresses the post-buckling analysis of a simply-supported symmetric cross-ply [0°/90°/0°] beam structure. For the purpose of illustration, each layer is made of an orthotropic material with properties as follows: $E_1 = 155$ GPa, $E_2 = 15.5$ GPa, $G_{12} = G_{13} = 0.6\,E_2$, $G_{23} = 0.5\,E_2$, $\nu_{12} = 0.25$. The beam cross-section is square with width $b = 5$ mm and total height $h = b$. In addition, each layer of the laminate has the same thickness $t = h/3$ and the length-to-width ratio L/b is set to be equal to 50, where L is the beam length.

Before comparing the numerical results of various geometrically nonlinear approximations, we first carry out the comparison based on different expansion functions on the cross-section

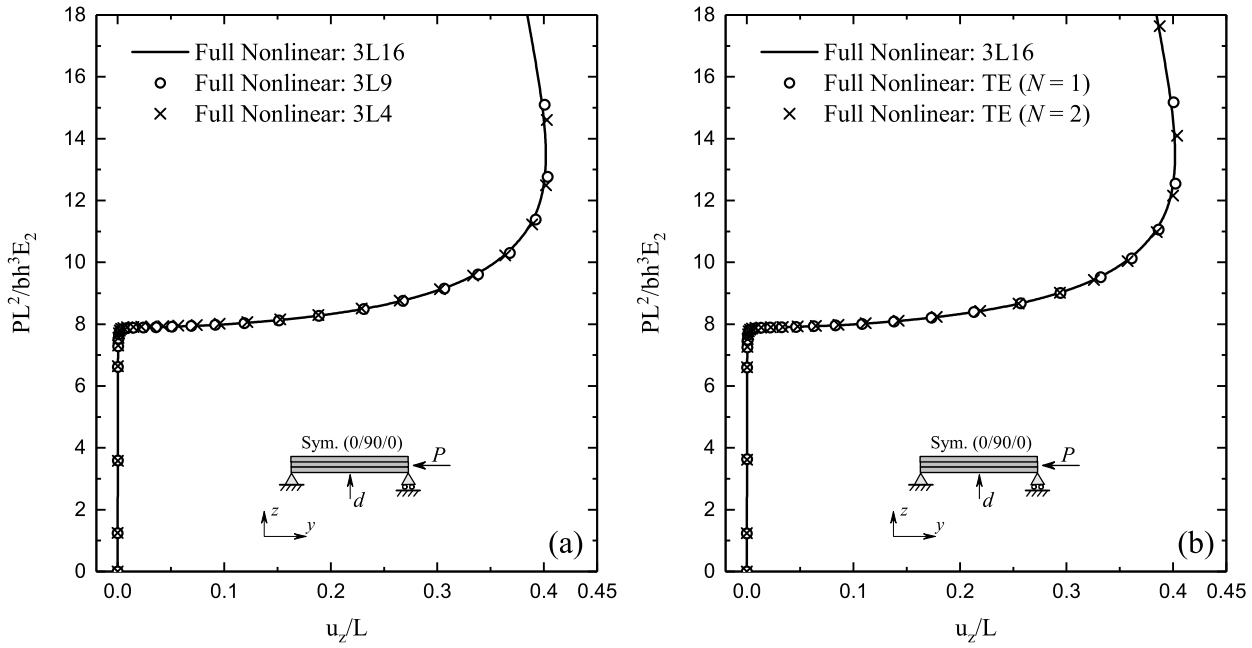

Figure 2: Post-buckling equilibrium curves of the simply-supported symmetric cross-ply [0°/90°/0°] beam (L = 250 mm, b = 5 mm): (a) comparison of different LE functions; (b) comparison of L16 with different TE functions.

(i.e. various kinematics). Specifically, we calculate the post-buckling equilibrium curves of the simply-supported symmetric cross-ply beam in Fig. 2 for different LE and TE functions, where the applied compression load P at the tip end varies with the vertical displacement component u_z at the center of the mid-span section. The loading and boundary conditions are also shown in Fig. 2 for clarity reasons, where a small defect load $d = 0.2$ N is applied at the mid-span section to *activate* the stable branch along the nonlinear response path. These solutions provided by the bi-linear (3L4), bi-quadratic (3L9), and bi-cubic (3L16) layer-wise full nonlinear CUF models are compared in Fig. 2(a), while the numerical results predicted by the TE functions ($N = 1$ and $N = 2$) and the bi-cubic layer-wise LE function (3L16) based on the full geometrically nonlinear theory are depicted in Fig. 2(b). Furthermore, the normalized axial stress σ_{yy} and transverse stress σ_{yz} distributions along the thickness of the laminated beam close to the loaded end (at $y = 0.9\,L$) is demonstrated in Fig. 3 for different cross-section kinematics based on the 3D full nonlinear theory at a fixed loading force $PL^2/(bh^3E_2) = 10$.

It should be pointed out from Figs. 2 and 3 that (1) both lower- and higher-order LE and TE full geometrically nonlinear CUF models can be able to correctly predict the post-buckling equilibrium path and capture successfully the reliable axial stress distribution of the simply-supported symmetric cross-ply beam; (2) in order to accurately describe the quadratic piece-wise distributions of the transverse shear stresses and ensure the continuity of the shear stresses through the thickness in the large-deflection and post-buckling regime (which is required physically), the bi-cubic layer-wise LE function (3L16) based on the 3D full nonlinear theory is needed. On the contrary, other kinematics can only predict constant or linear distributions of the shear stresses. Post-buckling equilibrium curves and stress distributions have also been calculated for various length-to-width ratios. The results are qualitatively similar to those in Figs. 2 and 3 and thus not reported here for the sake of brevity.

As a result, in the following calculations, we will exploit the bi-cubic layer-wise LE kinematics (L16) as a basis to assess the validation ranges of different geometrically nonlinear

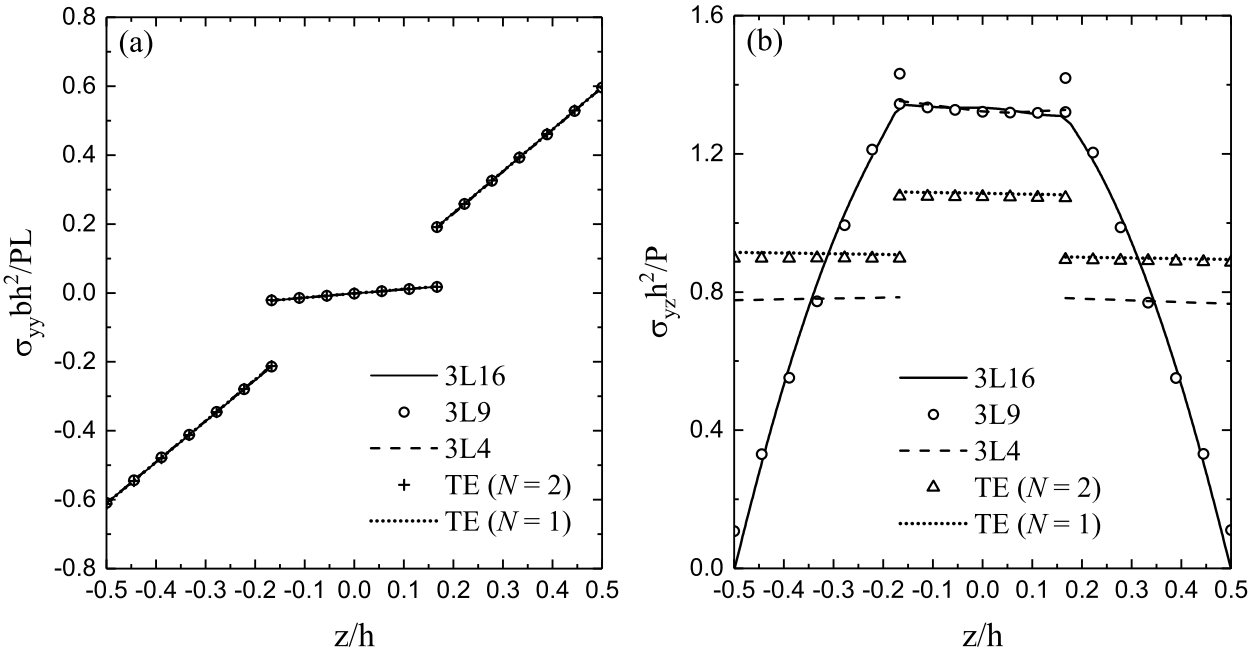

Figure 3: Through-the-thickness distributions of the normalized components of axial stress σ_{yy} (a) and transverse stress σ_{yz} (b) at $y = 0.9\,L$ of the simply-supported symmetric cross-ply [0°/90°/0°] beam ($L = 250$ mm, $b = 5$ mm, and $PL^2/(bh^3E_2) = 10$).

approximations, since the numerical results for the L16 full nonlinear CUF model can be assumed to be highly accurate [45].

To clearly highlight the difference predicted by different geometrically nonlinear approximations, the post-buckling equilibrium curves of the simply-supported symmetric cross-ply [0°/90°/0°] beam are displayed in Fig. 4 for various geometrically nonlinear models. In essence, different nonlinear terms of the operator matrix $\mathbf{b}_{nl}$ are activated in each geometrically nonlinear approximation theory. For instance, the analysis with all 3D nonlinear terms involved (i.e., 3D full Green-Lagrange strains are included) is hereafter abbreviated as the "Full Nonlinear" analysis, while that with all nonlinear terms excluded represents a "Linear" analysis that predicts a vertical straight line in Fig. 4, meaning that a Linear analysis cannot generate the buckling phenomenon. It is worth pointing out that since the bending and buckling of the structure is enforced in the $y - z$ plane by a small defect load acting in the z-direction, the nonlinear terms including the derivatives with respect to x and being associated with the displacement u_x have little influence on the nonlinear response of the structure. Therefore, the result of this analysis excluding those nonlinear terms shows the same trend of the"Full Nonlinear" analysis and hence is omitted here. The "1D-VK" analysis in Fig. 4 utilizes the von Kármán assumptions to 1D beams with the only non-zero nonlinear strain term $\mathbf{b}_{nl}[2,3]$, presented in Eq. (8). It can be seen from Fig. 4 that an almost horizontal line after the buckling load is predicted based on the 1D-VK analysis, which will deviate from the Full Nonlinear solution around the normalized displacement value of $u_z/L = 0.075$. In addition, the 1D-VK analysis overestimates the transverse displacements for a given loading force, especially in the advanced nonlinear regime. This phenomenon is qualitatively similar to that observed by Kim and Chaudhuri [43] in the geometrically nonlinear analysis of laminated cylindrical panels. It is important to notice that in order to fulfill the compatibility between the von Kármán strains and the model kinematics, the nonlinear effects of all shear strains along with the bending need to be considered (i.e., the nonlinear term $\mathbf{b}_{nl}[3,2]$ should be

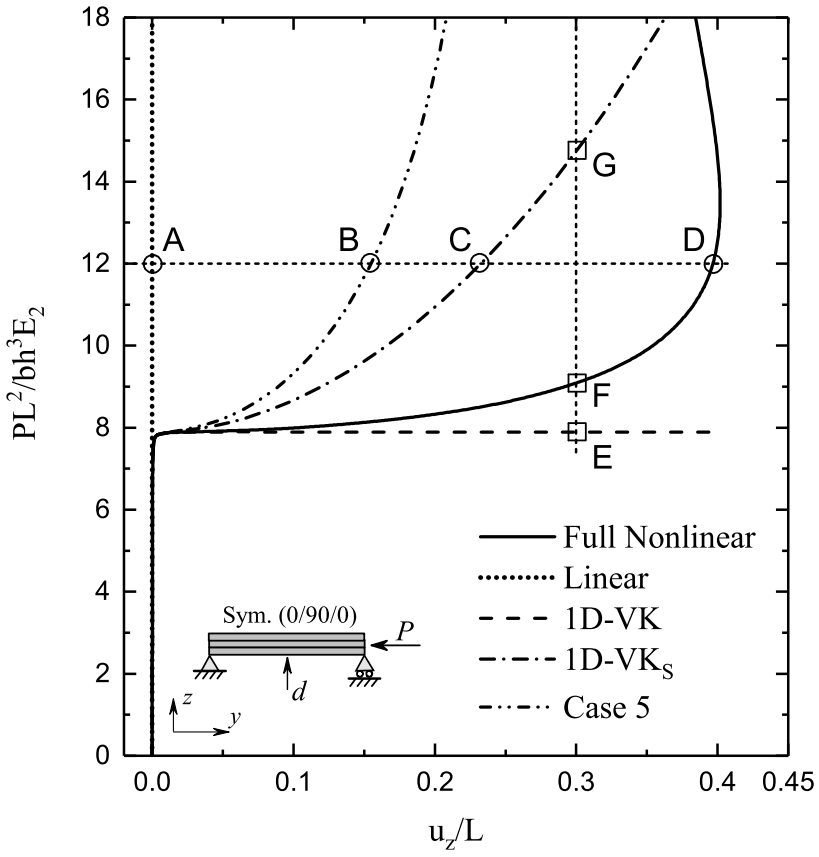

Figure 4: Post-buckling equilibrium curves of the simply-supported symmetric cross-ply [0°/90°/0°] beam (L = 250 mm, b = 5 mm) subjected to compression based on different geometrically nonlinear theories.

also taken into account in addition to $\mathbf{b}_{nl}[2,3]$). The analysis with all nonlinear shear effects will be referred to as "1D-VK$_S$" afterwards for simplicity. Fig. 4 shows that both 1D-VK$_S$ and 1D-VK curves can capture the buckling conditions, but after that, the 1D-VK$_S$ analysis describes a more rigid structure, which physically means that a higher compression loading predicted by the 1D-VK$_S$ analysis is needed to reach the same displacement than that by the 1D-VK theory. In order to demonstrate how the post-buckling equilibrium curve can change if other nonlinear terms are chosen, we show the final analysis "Case 5" in Fig. 4, where the nonlinear terms $\mathbf{b}_{nl}[2,2]$, $\mathbf{b}_{nl}[2,3]$, $\mathbf{b}_{nl}[3,2]$, $\mathbf{b}_{nl}[3,3]$ and $\mathbf{b}_{nl}[5,2]$ are included. In a word, the validation range predicted by the 1D-VK analysis is largest compared with other nonlinear approximation theories, but there is no solution to the nonlinear response for the 1D-VK analysis when the compression loading exceeds the buckling load.

Furthermore, the through-the-thickness distributions of the normalized axial stress σ_{yy} and transverse shear stress σ_{yz} components at $y = 0.9\,L$ of the simply-supported symmetric cross-ply [0°/90°/0°] beam are depicted in Fig. 5 based on different geometrically nonlinear theories. Figs. 5(a) and 5(b) show the stress distributions of equilibrium points A, B, C and D shown in Fig. 4 for a fixed loading force $PL^2/(bh^3E_2) = 12$, while Figs. 5(c) and 5(d) display the stress distributions of equilibrium points E, F, G and the Case 5 analysis shown in Fig. 4 for a fixed displacement $u_z/L = 0.3$. Note that the transverse stress σ_{yz} distribution corresponding to the Case 5 is not shown in Fig. 5(d) since its predicting result is much larger than those given by other nonlinear approximation theories.

It can be seen from Figs. 5(a) and 5(c) that the Full Nonlinear prediction gives the linear

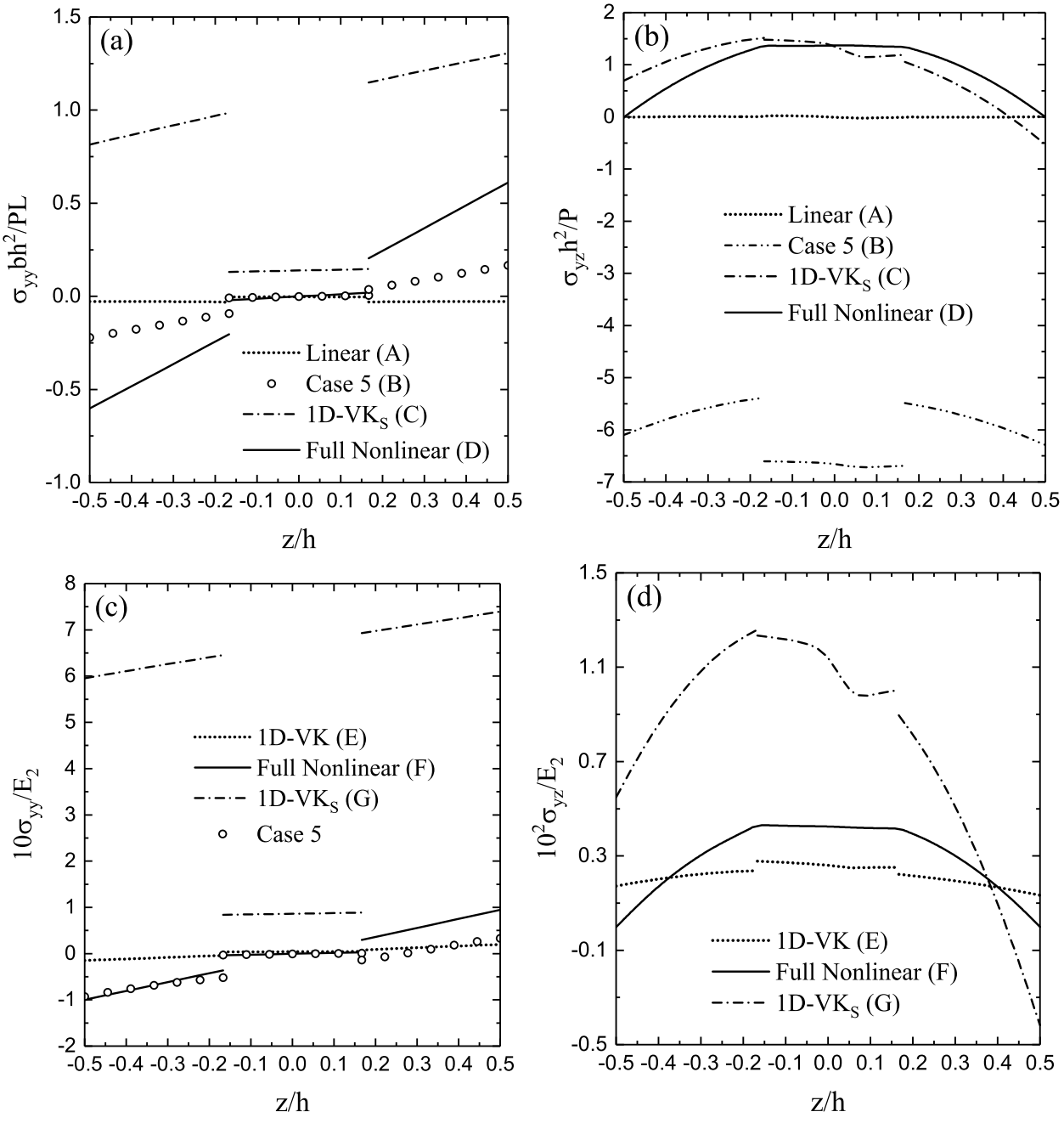

Figure 5: Through-the-thickness distributions of the normalized components of axial stress σ_{yy} (a, c) and transverse shear stress σ_{yz} (b, d) based on different geometrically nonlinear theories at $y = 0.9\,L$ of the simply-supported symmetric cross-ply [0°/90°/0°] beam ($L = 250$ mm, $b = 5$ mm): (a, b) for a fixed loading force $PL^2/(bh^3E_2) = 12$ corresponding to points A, B, C and D shown in Fig. 4; (c, d) for a fixed displacement $u_z/L = 0.3$ corresponding to points E, F, G and the Case 5 shown in Fig. 4.

axial stress distribution and clearly demonstrates the flexure nature of the symmetric structure after the buckling phenomenon occurs. However, other approximation theories deviate largely from the Full Nonlinear results. In particular, the 1D-VK$_S$ model induces the positive axial stress along the whole thickness of the laminated beam, which violates the intrinsic flexure characteristics and is unacceptable physically. As described above, the 3L16 Full Nonlinear analysis can accurately predict the quadratic transverse shear stress distribution and the continuity of the shear stress through the thickness, shown in Figs. 5(b) and 5(d). Nonetheless, other nonlinear assumption models cannot ensure the continuous transverse shear stress distributions.

The displacements at the mid-span cross-section and the deformed configurations of the simply-supported symmetric cross-ply [0°/90°/0°] beam based on different geometrically nonlinear approximation theories for a fixed loading force $PL^2/(bh^3E_2) = 12$ are depicted in Table 1. It is worth noticing that corresponding to the loading case, no solution for the 1D-VK analysis exists for the nonlinear response. The Full Nonlinear analysis predicts the largest mid-span displacement and describes the most compliant structure. Additionally, Table 2 displays the loading forces and the deformed configurations of the simply-supported symmetric cross-ply [0°/90°/0°] beam based on different geometrically nonlinear theories for a fixed mid-span displacement $u_z/L = 0.3$. Although the mid-span displacements are the same for different analyses, the deformed modes of the whole structure are different from each other.

	Linear (A)	Case 5 (B)	1D-VK$_S$ (C)	Full Nonlinear (D)
Displacement at the mid-span	$u_z = 0.008$	$u_z = 39.335$	$u_z = 58.517$	$u_z = 99.473$
Deformed Configuration (x-direction view)				

Table 1: Displacements at the mid-span and deformed configurations of the simply-supported symmetric cross-ply [0°/90°/0°] beam based on different geometrically nonlinear theories for a fixed loading force $PL^2/(bh^3E_2) = 12$ (i.e., $P = 1.86 \times 10^3$ N) corresponding to points A, B, C and D shown in Fig. 4. Note: u_z is expressed in mm.

	1D-VK (E)	Full Nonlinear (F)	1D-VK$_S$ (G)	Case 5
Loading Force	$P = 1.224$	$P = 1.406$	$P = 2.280$	$P = 10.894$
Deformed Configuration (x-direction view)				

Table 2: Loading forces and deformed configurations of the simply-supported symmetric cross-ply [0°/90°/0°] beam based on different geometrically nonlinear theories for a fixed mid-span displacement $u_z/L = 0.3$ (i.e., $u_z = 75$ mm) corresponding to points E, F, G and the Case 5 shown in Fig. 4. Note: P is expressed in 10^3 N.

Now we turn to investigating the effect of different lamination angles on the buckling and

post-buckling characteristics. In the case of simply-supported boundary conditions, the post-buckling equilibrium curves of three-layered composite beams for different lamination angles are plotted in Fig. 6 based on the Full Nonlinear analysis. It should be emphasized that for the asymmetric cross-ply beams such as $[-15°/0°/15°]$ and $[-45°/0°/45°]$, a small defect load applied at the mid-span is still required to *induce* the post-buckling branch. It can be seen from Fig. 6 that the variation trend of the post-buckling equilibrium curves is not qualitatively affected by the lamination angle, but the lamination angle indeed has a significant influence on the buckling loads of three-layered composite beams and must be taken into account. Specifically, the normalized critical buckling loads $P_{cr}L^2/(bh^3E_2)$ correponding to $[0°/90°/0°]$, $[-15°/0°/15°]$, $[-45°/0°/45°]$, $[45°/90°/45°]$ and $[-90°/0°/90°]$ laminated beams are about 7.88, 4.90, 1.50, 1.25 and 1.10. Thus, the symmetric cross-ply $[0°/90°/0°]$ beam structure can withstand larger loads before buckling due to the more rigid outer layers along the axial direction. Finally, it can be noted from Fig. 6 that the post-buckling equilibrium curves of the $[-45°/0°/45°]$ and $[-90°/0°/90°]$ laminated beams overlap with the $[45°/0°/45°]$ and $[90°/0°/90°]$ laminated beams, which can be assumed trivial owing to the relation $\cos\theta = \cos(-\theta)$.

For three-layered composite beams with simply-supported boundary conditions and different lamination angles from $[0°/90°/0°]$, we have also numerically calculated the post-buckling equilibrium curves for various geometrically nonlinear theories. The qualitative variation trend is unaltered compared with that in Fig. 4 and thus not reported here.

5.2 Large-deflection of two-layered asymmetric composite beams

Now our interest is to employ the 3D full geometrically nonlinear CUF model to determine the validation ranges of different geometrically nonlinear assumptions for two-layered asymmetric composite beams subjected to compression loadings. For representative purposes, we will first consider the two-layered asymmetric $[0°/45°]$ beam structure and each layer has the same thickness $t = h/2 = 0.3$ m. The total length and section width of the laminated beam are equal to $L = 9$ m and $b = 1$ m, respectively. Besides, the laminated beam consists of an orthotropic AS4/3501-6 graphite/epoxy material with the following properties: $E_1 = 144.8$ GPa, $E_2 = 9.65$ GPa, $G_{12} = G_{13} = 4.14$ GPa, $G_{23} = 3.45$ GPa, $\nu_{12} = 0.3$.

Fig. 7 demonstrates the post-buckling equilibrium curves of the cantilever asymmetric cross-ply $[0°/45°]$ composite beam subjected to compression for various geometrically nonlinear models including the Linear, 1D-VK, 1D-VK$_S$, Case 5 and Full Nonlinear analyses. The post-buckling equilibrium curves provide the vertical displacement component u_z as functions of the applied compression load P. Note that the displacements are calculated at the free end of the cantilever beam and the Full Nonlinear analysis is based on the 2L16 layer-wise CUF beam model. For the sake of clarity, the loading and boundary conditions are also displayed in Fig. 7, and there is no need to apply the defect load. As we can see, due to the coupling effect between the axial and transverse displacement components, the Linear analysis generates an *almost* vertical straight line and the predicted displacement is extremely small. It can be found from Fig. 7 that the predictions of the 1D-VK analysis with the classical von Kármán approximations and of the Full Nonlinear analysis are almost indistinguishable when $u_z/L \leq 0.2$. However, when $u_z/L > 0.2$, the difference between them gradually increases. Specifically, the 1D-VK analysis predicts an almost horizontal line and overestimates the transverse displacements for a given loading force [43], which is similar to that in Fig. 4. The post-buckling curves predicted by the 1D-VK$_S$ analysis with modification to include nonlinear shear effects and by the Case 5 analysis begin to deviate from that based on the Full

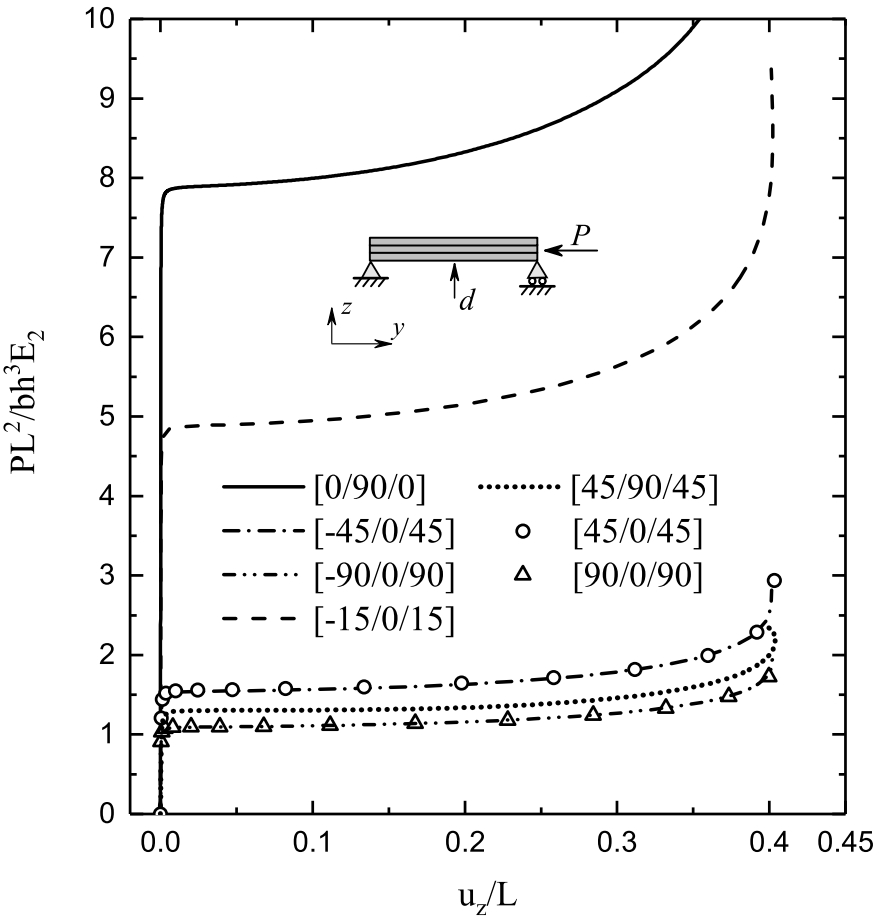

Figure 6: Post-buckling equilibrium curves of three-layered simply-supported composite beams ($L = 250$ mm, $b = 5$ mm) for different lamination angles based on the Full Nonlinear analysis.

Nonlinear analysis after the normalized displacement value of 0.1. Consequently, the validation range of the latter two nonlinear approximation theories is smaller than that of the 1D-VK analysis, which cannot provide solutions to the nonlinear response after approximately $PL^2/(bh^3E_2) = 0.74$.

Moreover, Fig. 8 shows through-the-thickness distributions of the normalized axial stress σ_{yy} and transverse shear stress σ_{yz} components at the mid-span section of the cantilever asymmetric cross-ply [0°/45°] beam based on different geometrically nonlinear theories. Specifically, the stress distributions of equilibrium points A, B, C and D labelled in Fig. 7 for a fixed compression load $PL^2/(bh^3E_2) = 0.9$ are displayed in Figs. 8(a) and 8(b), while Figs. 8(c) and 8(d) depict the stress distributions of equilibrium states E, F, G and the Case 5 analysis in Fig. 7 for a fixed vertical displacement $u_z/L = 0.55$. It can be found from Figs. 8(a) and 8(c) that although all the geometrically nonlinear approximation theories predict linear axial stress distributions along the beam thickness, their predictions deviate quantitatively from the Full Nonlinear results. In addition, analogous to the symmetric cross-ply [0°/90°/0°] beam case shown in Figs. 5(b) and 5(d), the 2L16 Full Nonlinear analysis in Figs. 8(b) and 8(d) can ensure the continuity of the transverse shear stress and result into the quadratic shear stress distributions. Interestingly, it can be found from Figs. 8(b) and 8(d) that the prediction results based on the 1D-VK$_S$ analysis also display the continuous shear stress distributions owing to the correction of nonlinear shear strain effects. Other nonlinear approximation the-

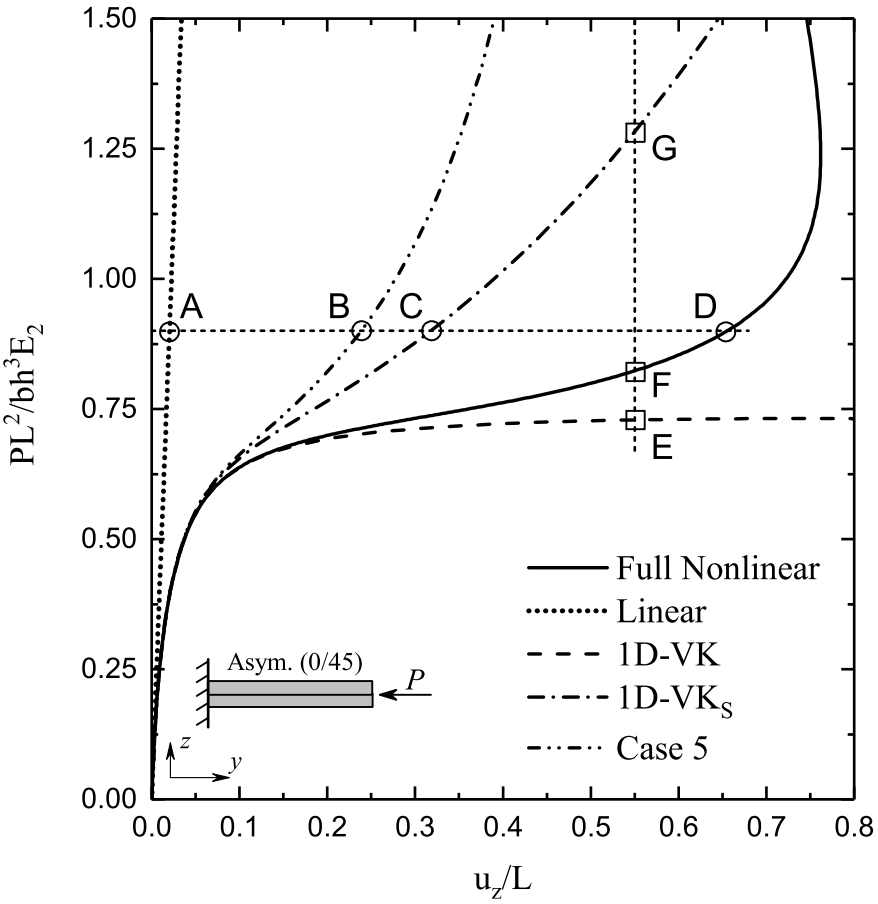

Figure 7: Post-buckling equilibrium curves of the cantilever asymmetric cross-ply [0°/45°] composite beam ($L = 9$ m, $b = 1$ m) subjected to compression based on different geometrically nonlinear theories.

ories cannot guarantee the continuous transverse stress distributions. Therefore, the Full Nonlinear analysis is of paramount importance to predict the accurate stress distributions in the large-deflection scenario.

In order to evidently demonstrate the equilibrium states of different geometrically nonlinear theories, Table 3 concludes and compares the displacements at the free end and the deformed configurations of the cantilever asymmetric cross-ply [0°/45°] beam for a fixed loading force $PL^2/(bh^3E_2) = 0.9$. Similar to the results in Table 1, the 2L16 Full Nonlinear analysis leads to the largest displacement at the free end. In addition, Table 4 shows the loading forces and the deformed configurations of the cantilever asymmetric cross-ply [0°/45°] beam based on different geometrically nonlinear theories for a fixed free-end displacement $u_z/L = 0.55$. It can be noted that the deformed modes of the laminated beam differ from each other.

Finally, Fig. 9 displays the post-buckling equilibrium curves of the cantilever asymmetric cross-ply [0°/90°] and [15°/ − 45°] laminated beams subjected to the compression load based on various geometrically nonlinear theories. The numerical results and discussion procedure are qualitatively analogous to those in Fig. 7 and hence neglected here for simplicity. It can be seen that the variation trend of the post-buckling equilibrium curves hardly varies with the stacking sequence of the two-layered asymmetric composite beams.

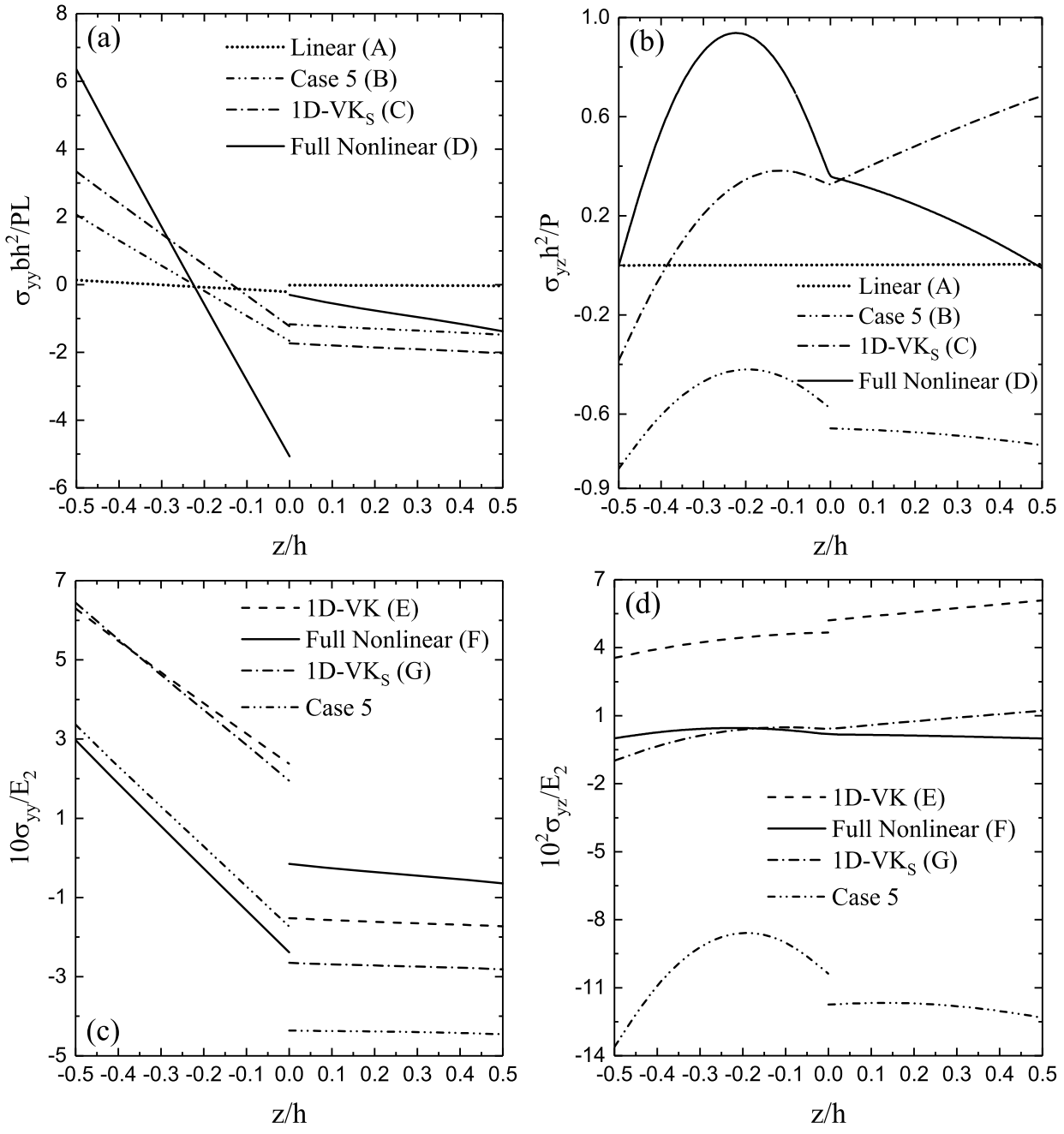

Figure 8: Through-the-thickness distributions of the normalized components of axial stress σ_{yy} (a, c) and transverse shear stress σ_{yz} (b, d) based on different geometrically nonlinear theories at the mid-span of the cantilever asymmetric cross-ply [0°/45°] beam: (a, b) for a fixed loading force $PL^2/(bh^3E_2) = 0.9$ corresponding to points A, B, C and D shown in Fig. 7; (c, d) for a fixed displacement $u_z/L = 0.55$ corresponding to points E, F, G and the Case 5 shown in Fig. 7.

	Linear (A)	Case 5 (B)	1D-VK$_S$ (C)	Full Nonlinear (D)
Displacement at the free end	$u_z = 0.182$	$u_z = 2.169$	$u_z = 2.881$	$u_z = 5.951$
Deformed Configuration (x-direction view)				

Table 3: Displacements at the free end and deformed configurations of the cantilever asymmetric cross-ply [0°/45°] beam based on different geometrically nonlinear theories for a fixed loading force $PL^2/(bh^3E_2) = 0.9$ (i.e., $P = 2.316 \times 10^7$ N) corresponding to points A, B, C and D shown in Fig. 7. Note: u_z is expressed in m.

	1D-VK (E)	Full Nonlinear (F)	1D-VK$_S$ (G)	Case 5
Loading Force	$P = 1.877$	$P = 2.112$	$P = 3.276$	$P = 10.975$
Deformed Configuration (x-direction view)				

Table 4: Loading forces and deformed configurations of the cantilever asymmetric cross-ply [0°/45°] beam based on different geometrically nonlinear theories for a fixed tip end displacement $u_z/L = 0.55$ (i.e., $u_z = 4.95$ m) corresponding to points E, F, G and the Case 5 shown in Fig. 7. Note: P is expressed in 10^7 N.

6 Conclusions

In this paper, we accurately determined the stress field distributions for the large-deflection and post-buckling of laminated composite beams based on various geometrically nonlinear approximations. We briefly addressed the formulations utilized to conduct such investigations, which is based on the Carrera Unified Formulation (CUF). Specifically, the nonlinear governing equations along with the related finite element approximation have been presented and formulated employing the principle of virtual work. We provided a detailed numerical evaluation for the post-buckling of three-layered composite beams and for the large displacement analysis of two-layered asymmetric composite beams under compression, in order to quantitatively compare the numerical results of various cross-sectional kinematics (including both TE and LE) and different geometrically nonlinear models (including 3D full nonlinear model, 1D von Kármán approximation and its modified counterpart with nonlinear shear effects). Owing to the scalable advantage of CUF, we can consistently investigate the effects of different geometrically nonlinear approximations in a unified way, without altering the form of CUF. From the numerical results, we can draw the following conclusions:

1) For symmetric cross-ply beams, both TE and LE 3D full geometrically nonlinear CUF models can correctly predict the post-buckling equilibrium curves and successfully capture the reliable *axial* stress distributions. Nevertheless, in order to accurately describe the quadratic piece-wise distributions of the *transverse shear* stresses and ensure their continuity through the thickness in the case of large-deflection and post-buckling, the bi-cubic layer-wise LE function based on the Full Nonlinear theory is required with high accuracy,

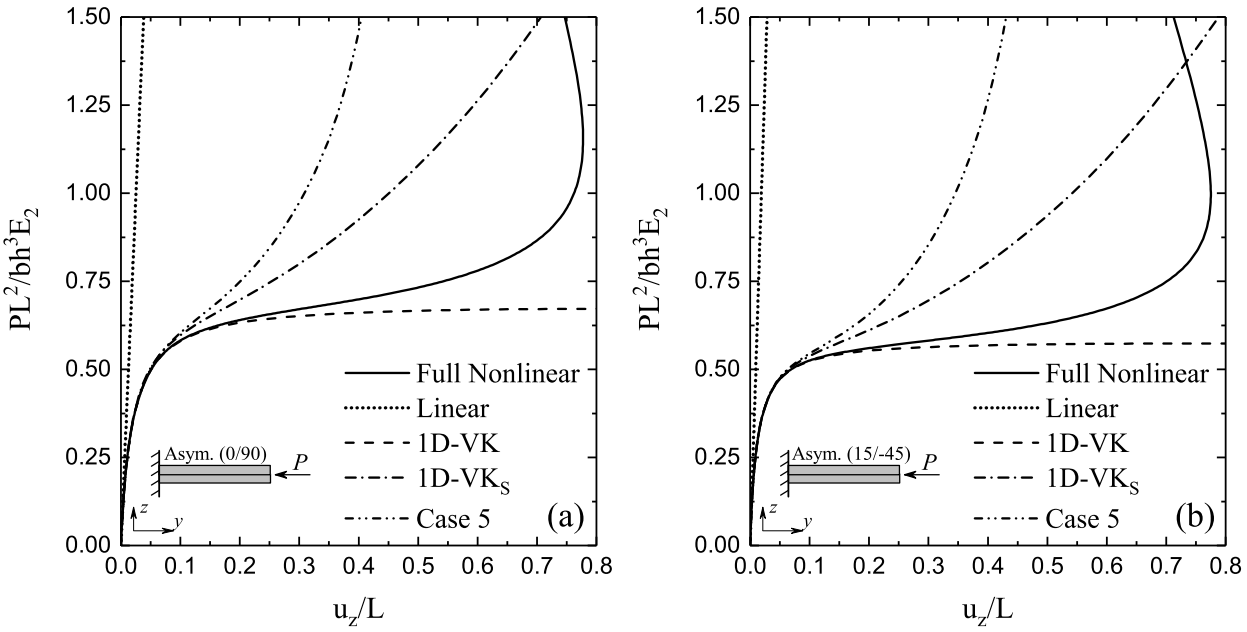

Figure 9: Post-buckling equilibrium curves of the cantilever asymmetric composite beam ($L = 9$ m, $b = 1$ m) subjected to compression based on different geometrically nonlinear theories: (a) $[0°/90°]$; (b) $[15°/-45°]$.

which could be a basis to assess the validation ranges of different geometrically nonlinear approximations.

2) Geometrically nonlinear simplified models such as the von Kármán model may provide acceptable results of the post-buckling equilibrium curves in the regimes of small and moderate displacements/rotations, while, in the large displacement/rotation analysis, the 3D full geometrically nonlinear CUF model must be exploited to obtain the reliable results.

3) Full Nonlinear predictions yield the *linear axial* stress distributions and clearly demonstrate the flexure nature subjected to the compression loading, while other approximation theories deviate largely from the Full Nonlinear results. Unlike the bi-cubic layer-wise LE Full Nonlinear model, most of other geometrically nonlinear approximation models cannot describe the continuous transverse shear stress distributions.

4) The lamination angle or the stacking sequence does not qualitatively affect the variation trend of the post-buckling equilibrium curves, but it indeed has a significant influence on the buckling loads of laminated composite beams.

All these results provide significant guidance for the accurate analysis of the post-buckling equilibrium curves and the stress field distributions for the geometrically nonlinear laminated composite beams. In addition, the validation ranges of various geometrically nonlinear approximation models can be determined compared with the 3D full geometrically nonlinear model.

Finally, we emphasize here that in the large-deflection and post-buckling analyses investigated in this work, only the geometrical nonlinearity is taken into consideration and the flexible composites are assumed to be linear elastic under the assumption of small strains. For biological soft materials commonly subjected to large strains (or deformations), further analysis on the influence of both geometrical and material nonlinearities on the stress field

distributions for the large-deflection and post-buckling of laminated composites should be required, especially for incompressible biological hyperelastic materials [4, 61].

References

[1] E. Carrera. Historical review of zig-zag theories for multilayered plates and shells. *Applied Mechanics Reviews*, 56(3):287–308, 2003.

[2] R. K. Kapania and S. Raciti. Recent advances in analysis of laminated beams and plates. Part I: Shear effects and buckling. *AIAA Journal*, 27(7):923–935, 1989.

[3] R. K. Kapania and S. Raciti. Recent advances in analysis of laminated beams and plates, Part II: Vibrations and wave propagation. *AIAA Journal*, 27(7):935–946, 1989.

[4] M. Amabili. *Nonlinear Mechanics of Shells and Plates in Composite, Soft and Biological Materials*. Cambridge University Press, New York, USA, 2018.

[5] L. Euler. *De curvis elasticis*. Lausanne and Geneva: Bousquet, 1744.

[6] S. P. Timoshenko. On the transverse vibrations of bars of uniform cross-section. *Philosophical Magazine*, 43(253):125–131, 1922.

[7] N. J. Pagano. Exact solutions for composite laminates in cylindrical bending. *Journal of Composite Materials*, 3(3):398–411, 1969.

[8] J. N. Reddy. A simple higher-order theory for laminated composite plates. *Journal of Applied Mechanics*, 51(4):745–752, 1984.

[9] S. R. Marur and T. Kant. Transient dynamics of laminated beams: An evaluation with a higher-order refined theory. *Composite Structures*, 41(1):1–11, 1998.

[10] T. Kant and K. Swaminathan. Analytical solutions for the static analysis of laminated composite and sandwich plates based on a higher order refined theory. *Composite Structures*, 56(4):329–344, 2002.

[11] E. Carrera and A. Ciuffreda. A unified formulation to assess theories of multilayered plates for various bending problems. *Composite Structures*, 69(3):271–293, 2005.

[12] E. Carrera and M. Petrolo. Refined beam elements with only displacement variables and plate/shell capabilities. *Meccanica*, 47(3):537–556, 2012.

[13] E. Carrera and M. Petrolo. Refined one-dimensional formulations for laminated structure analysis. *AIAA Journal*, 50(1):176–189, 2012.

[14] M. Filippi and E. Carrera. Various refined theories applied to damped viscoelastic beams and circular rings. *Acta Mechanica*, 228(12):4235–4248, 2017.

[15] E Carrera and B Kröplin. Zigzag and interlaminar equilibria effects in large-deflection and postbuckling analysis of multilayered plates. *Mechanics of Composite Materials and Structures*, 4(1):69–94, 1997.

[16] N. J. Pagano and S. J. Hatfield. Elastic behavior of multilayered bidirectional composites. *AIAA Journal*, 10(7):931–933, 1972.

[17] J. N. Reddy. *Mechanics of Laminated Composite Plates and Shells: Theory and Analysis*. CRC Press, 2004.

[18] H. Murakami. Laminated composite plate theory with improved in-plane responses. *Journal of Applied Mechanics*, 53(3):661–666, 1986.

[19] E. Carrera. On the use of the Murakami's zig-zag function in the modeling of layered plates and shells. *Computers & Structures*, 82(7-8):541–554, 2004.

[20] E. Reissner. On a certain mixed variational theorem and a proposed application. *International Journal for Numerical Methods in Engineering*, 20(7):1366–1368, 1984.

[21] E. Reissner. On a mixed variational theorem and on shear deformable plate theory. *International Journal for Numerical Methods in Engineering*, 23(2):193–198, 1986.

[22] E. Carrera. C^0 Reissner–Mindlin multilayered plate elements including zig-zag and interlaminar stress continuity. *International Journal for Numerical Methods in Engineering*, 39(11):1797–1820, 1996.

[23] Robbins Jr. D. H. and J. N. Reddy. Modelling of thick composites using a layerwise laminate theory. *International Journal for Numerical Methods in Engineering*, 36(4):655–677, 1993.

[24] L. Vu-Quoc, H. Deng, and X. G. Tan. Geometrically-exact sandwich shells: The static case. *Computer Methods in Applied Mechanics and Engineering*, 189(1):167–203, 2000.

[25] Y. Başar, M. Itskov, and A. Eckstein. Composite laminates: Nonlinear interlaminar stress analysis by multi-layer shell elements. *Computer Methods in Applied Mechanics and Engineering*, 185(2-4):367–397, 2000.

[26] E. Carrera. Evaluation of layerwise mixed theories for laminated plates analysis. *AIAA Journal*, 36(5):830–839, 1998.

[27] E. M. Austin and D. J. Inman. A C^1 finite element capable of interlaminar stress continuity. *Computers & Structures*, 79(10):973–986, 2001.

[28] W. J. Liou and C. T. Sun. A three-dimensional hybrid stress isoparametric element for the analysis of laminated composite plates. *Computers & Structures*, 25(2):241–249, 1987.

[29] T. H. H. Pian and C. C. Wu. *Hybrid and Incompatible Finite Element Methods*. Chapman & Hall, CRC, 2005.

[30] C. H. Zhang and S. V. Hoa. A systematic and quantitative method to determine the optimal assumed stress fields for hybrid stress finite elements. *Finite Elements in Analysis and Design*, 80:41–62, 2014.

[31] L. Vu-Quoc and X. G. Tan. Efficient hybrid-eas solid element for accurate stress prediction in thick laminated beams, plates, and shells. *Computer Methods in Applied Mechanics and Engineering*, 253:337–355, 2013.

[32] H. B. Coda. Continuous inter-laminar stresses for regular and inverse geometrically non linear dynamic and static analyses of laminated plates and shells. *Composite Structures*, 132:406–422, 2015.

[33] R. Carrazedo and H. B. Coda. Triangular based prismatic finite element for the analysis of orthotropic laminated beams, plates and shells. *Composite Structures*, 168:234–246, 2017.

[34] H. B. Coda, R. R. Paccola, and R. Carrazedo. Zig-zag effect without degrees of freedom in linear and non linear analysis of laminated plates and shells. *Composite Structures*, 161:32–50, 2017.

[35] G. V. Nogueira, R. R. Paccola, and H. B. Coda. A positional unconstrained vector layerwise (UVLWT) fem formulation for laminated frame element modeling. *Composite Structures*, 148:97–112, 2016.

[36] R. K. Kapania and S. Raciti. Nonlinear vibrations of unsymmetrically laminated beams. *AIAA Journal*, 27(2):201–210, 1989.

[37] G. Singh, G. V. Rao, and N. G. R. Iyengar. Nonlinear bending of thin and thick unsymmetrically laminated composite beams using refined finite element model. *Computers & Structures*, 42(4):471–479, 1992.

[38] W. B. Yu, D. H. Hodges, V. V. Volovoi, and E. D. Fuchs. A generalized Vlasov theory for composite beams. *Thin-Walled Structures*, 43(9):1493–1511, 2005.

[39] P. Vidal and O. Polit. Assessment of the refined sinus model for the non-linear analysis of composite beams. *Composite Structures*, 87(4):370–381, 2009.

[40] R. K. Gupta, J. B. Gunda, G. R. Janardhan, and G. V. Rao. Post-buckling analysis of composite beams: Simple and accurate closed-form expressions. *Composite Structures*, 92(8):1947–1956, 2010.

[41] S. A. Emam. Analysis of shear-deformable composite beams in postbuckling. *Composite Structures*, 94(1):24–30, 2011.

[42] E. Carrera and H. Parisch. An evaluation of geometrical nonlinear effects of thin and moderately thick multilayered composite shells. *Composite Structures*, 40(1):11–24, 1997.

[43] D. Kim and R. A. Chaudhuri. Full and von Kármán geometrically nonlinear analyses of laminated cylindrical panels. *AIAA Journal*, 33(11):2173–2181, 1995.

[44] A. Pagani and E. Carrera. Unified formulation of geometrically nonlinear refined beam theories. *Mechanics of Advanced Materials and Structures*, 25(1):15–31, 2018.

[45] A. Pagani and E. Carrera. Large-deflection and post-buckling analyses of laminated composite beams by Carrera Unified Formulation. *Composite Structures*, 170:40–52, 2017.

[46] E. Carrera, G. Giunta, and M. Petrolo. *Beam Structures: Classical and Advanced Theories*. John Wiley & Sons, 2011.

[47] E. Carrera, M. Cinefra, M. Petrolo, and E. Zappino. *Finite Element Analysis of Structures through Unified Formulation*. John Wiley & Sons, Chichester, West Sussex, UK, 2014.

[48] A. Pagani, M. Petrolo, G. Colonna, and E. Carrera. Dynamic response of aerospace structures by means of refined beam theories. *Aerospace Science and Technology*, 46:360–373, 2015.

[49] E. Carrera and A. Pagani. Free vibration analysis of civil engineering structures by component-wise models. *Journal of Sound and Vibration*, 333(19):4597–4620, 2014.

[50] M. Filippi and E. Carrera. Dynamic analyses of axisymmetric rotors through three-dimensional approaches and high-fidelity beam theories. *Journal of Vibration and Acoustics*, 139(6):061008, 2017.

[51] F. Miglioretti and E. Carrera. Application of a refined multi-field beam model for the analysis of complex configurations. *Mechanics of Advanced Materials and Structures*, 22(1-2):52–66, 2015.

[52] A. Pagani, R. Augello, and E. Carrera. Frequency and mode change in the large deflection and post-buckling of compact and thin-walled beams. *Journal of Sound and Vibration*, 432:88–104, 2018.

[53] O. O. Ochoa and J. N. Reddy. *Finite Element Analysis of Composite Laminates*. Kluwer Academic Publishers, Dordrecht, The Netherlands, 1992.

[54] P. F. Pai. *Highly Flexible Structures: Modeling, Computation, and Experimentation*. AIAA Education Series, AIAA, Reston, VA, 2007.

[55] A. L. Gol'Denveizer. *Theory of Elastic Thin Shells: Solid and Structural Mechanics*. Pergamon Press, 1961.

[56] K. J. Bathe. *Finite Element Procedure*. Prentice Hall, Upper Saddle River, New Jersey, USA, 1996.

[57] M. A. Crisfield. A fast incremental/iterative solution procedure that handles "snap-through". *Computers & Structures*, 13(1):55–62, 1981.

[58] M. A. Crisfield. An arc-length method including line searches and accelerations. *International Journal for Numerical Methods in Engineering*, 19(9):1269–1289, 1983.

[59] E. Carrera. A study on arc-length-type methods and their operation failures illustrated by a simple model. *Computers & Structures*, 50(2):217–229, 1994.

[60] O. C. Zienkiewicz and R. L. Taylor. *The Finite Element Method for Solid and Structural Mechanics*. Butterworth-Heinemann, Washington, 6th edition, 2005.

[61] M. Amabili, I.D. Breslavsky, and J.N. Reddy. Nonlinear higher-order shell theory for incompressible biological hyperelastic materials. *Computer Methods in Applied Mechanics and Engineering*, 346:841–861, 2019.